Advances in the Theory of Nonlinear Analysis and its Applications 8 (2024) No. 1, 01-16.
https://doi.org/10.17762/atnaa.v8.i1.368
Available online at https://atnaea.org/
Research Article

Advances in the Theory of Nonlinear Analysis and its Applications

ISSN: 2587-2648 Peer-Reviewed Scientific Journal

THE IMPACT OF FREQUENCY MODULATED SIGNALS ON VIBRATIONAL RESONANCE IN A POSITION DEPENDENT MASS SYSTEM

K. SUDDALAI KANNAN, T. SAINTA JOSTER, A. ZEENATH BAZEERA, V. CHINNATHAMBI, S. RAJASEKAR

Abstract. This paper examines the impact of frequency-modulated (FM) signals on vibrational resonance (VR) in a position-dependent mass (PDM)-Duffing oscillator system. FM signals are categorized into two types: narrow-band FM (NBFM) and wide-band FM (WBFM). We conduct a numerical study to analyze the effects of both FM signals on the system. The occurrence of VR is investigated not only based on signal parameters (g, ω, Ω) but also considering the contributions of PDM parameters (m_0, λ). In addition to various dynamic phenomena such as period-doubling bifurcation, reverse period-doubling bifurcation, chaos, and attractor crises, our numerical simulations reveal several noteworthy observations. These include the emergence of multiple resonance peaks, the absence of response amplitude decay, the presence of hysteresis, and a jump phenomenon induced by the FM signal. By delving into phase portraits, bifurcation diagrams, trajectory plots, and resonance plots, we elucidate the underlying resonance mechanisms and provide insights into the distinctive features of the resonance curve.

Mathematics Subject Classification (2010):37D45, 34C37, 34D10, 34A08, 37J20, 37C29
Key words and phrases: Position dependent mass system Frequency modulated signal Vibrational resonance Hysteresis Chaos

1. Introduction

Over the past two decades, significant attention has been directed towards signal processing in nonlinear systems. There are numerous methods for enhancing the response amplitude of a weak signal, with one of the most crucial approaches being vibrational resonance (VR). In VR, a bistable system is subjected to the influence of a biharmonic signal with vastly different frequencies. The concept of vibrational resonance (VR) was initially documented by Landa and McClintock [1] in a biharmonically driven bistable system when a substantial discrepancy exists between the frequencies $(\Omega \gg \omega)$ of the two driving forces. Subsequently, analytical investigations to confirm VR were conducted by Gitterman [2] and Blekhman and Landa [3]. Following these pioneering works, researchers have delved into the theoretical, numerical, and experimental exploration of this resonance in various nonlinear systems [4-10]. The examination of two-frequency signals holds

Received October 01, 2023; Accepted: June 18, 2024; Online: July 25, 2024.

significance in communication systems since low-frequency signals typically modulate high-frequency carrier signals. Furthermore, this concept finds application in numerous other domains of physics and biology, including laser physics [11], acoustics [12], neuroscience [13], and ionospheric physics [14]. High-frequency forces have also been noted for their practical importance, particularly in medical applications [15-18].

The phenomenon of mass variation concerning velocity, position, time, or a combination thereof is referred to as "varying mass." Systems with varying masses manifest in diverse fields, including semiconductor theory [19,20], rocket motion [21], raindrop behavior [22], the inversion potential for NH_3 in density theory [23], the accretion of planets and asteroids in the early solar system [24], and neutrino mass oscillators [25]. In position-dependent mass (PDM) systems, where the variable mass is specified in terms of its position, various types of mass variation functions have been explored [26,27]. In the classical framework, a position-dependent mass function $m(x)$ gives rise to "forces quadratic in velocity," resulting in nonlinear differential equations of motion within the Newtonian framework.

2. **Frequency Modulated Signals**

The Frequency Modulated (FM) signal is typically classified into two main types: Narrow Band FM (NBFM) and Wide Band FM (WBFM), also known as Broadband FM. NBFM signals are characterized by their narrower bandwidth. The modulation index (M_f) of an NBFM signal is typically small, usually less than one radian. Consequently, the spectrum of an NBFM signal comprises the carrier frequency and upper and lower sidebands. Mathematically, the NBFM signal can be expressed as follows:

$$S_1(t) = f(\cos\omega t - g\sin\Omega t\sin\omega t),\ \Omega >> \omega, \tag{1}$$

In this equation, f represents the amplitude of the low-frequency (ω) periodic signal, which is modulated by a high-frequency (Ω) periodic signal with amplitude g. NBFM signals find applications in FM mobile communications, including police wireless, ambulances, and taxicabs, among others. When the modulation index takes on a large value, the FM signal ideally contains the carrier and an infinite number of sidebands symmetrically positioned around the carrier. Such an FM signal has an infinite bandwidth and is referred to as the Wide Band FM (WBFM) signal. Mathematically, the WBFM signal can be represented as:

$$S_2(t) = f\sin(\omega t + g\sin\Omega t),\ \Omega >> \omega. \tag{2}$$

The modulation index of the WBFM signal typically exceeds 1. WBFM signals are commonly used in entertainment broadcasting applications, such as FM radio and TV. Notably, some researchers have employed this signal to investigate various nonlinear phenomena in specific nonlinear systems [28,29].

3. Classical description of the system

Consider a classical PDM systems described by the Lagrangian

$$L(x,\dot{x},t) = T - V(x) = \frac{1}{2}m(x)\dot{x}^2 - V(x), \tag{3}$$

where $T = \frac{1}{2}m(x)\dot{x}^2$ is the kinetic energy of the system, $V(x)$ is the system's potential and $m(x)$ is the position-dependent mass function with x being position at time t. The associated Lagrangian equation of motion can be written as

$$\frac{d}{dt}\left(\frac{\partial L}{\partial \dot{x}}\right) - \frac{\partial L}{\partial x} = \Phi, \tag{4}$$

where Φ accounts for all the external contributions to the motion from dissipative and driving forces, assumed here to be $\Phi = -\alpha\dot{x} + S(t)$, α is the damping coefficient and $S(t)$ is the frequency modulated signals ($S_1(t)$ and $S_2(t)$). Using Eq.(3) in Eq.(4), the equation of motion of damped and driven classical oscillator may be written as

$$m(x)\ddot{x} + \frac{1}{2}m'(x)\dot{x}^2 + \frac{dV(x)}{dx} = \Phi \tag{5}$$

The prime in Eq.(5) implies differentiation with respect to space variable x and the over dot indicates differentiation with respect to time. Among the various types of mass variation function, we use the following mass variation function in the present study

$$m(x) = \frac{m_0}{1+\lambda x^2}, \tag{6}$$

where m_0 is a constant mass, equivalent to the mass amplitude and λ is the strength of the spatial nonlinearity in mass. The mass function is originally proposed by Mathews and Lakshmanan [26] in relation to relativistic fields of elementary particles. It appears frequently in the modelling of diverse nonlinear mechanical systems [30-32]. Further in the following analysis, we consider a Duffing type oscillator potential, ie.,

$$V(x) = \frac{1}{2}\, m(x)\, \omega_0^2\, x^2 + \frac{1}{4}\, \beta\, x^4\,, \tag{7}$$

where ω_0 is the oscillator's natural frequency and β is the stiffness constant which plays the role of the nonlinear parameter.

From the above one can easily show that the equation of motion of the PDM-Duffing oscillator can be written as

$$m(x)\, \ddot{x} - m^2(x)x\gamma\lambda\dot{x}^2 + \alpha\dot{x} + m^2(x)\, \gamma\omega_0^2\, x + \beta x^3 = S(t), \tag{8}$$

where $\gamma = \frac{1}{m_0}$. When the strength of nonlinearity in mass is negligible, that is $\lambda = 0$, unit mass amplitude $m(0) = 1$ and $g = 0$, Eq.(8) reduces to the well known Duffing oscillator equation driven by FM signal. The physical system (Eq.8) describes a dual frequency operated gas bubble in which the

mass of the bubble depends on the radius of the bubble, which is a spatial coordinate [33]. By dividing Eq.(8) by $m(x)$ we express it as

$$\ddot{x} - m_0(1+\lambda x^2)^{-1}(\gamma\lambda\, x\dot{x}^2 - \gamma\omega_0^2 x) + \gamma(1+\lambda x^2)(\alpha\dot{x} + \beta x^3) = \gamma(1+\lambda x^2)S(t) \tag{9}$$

The term $(1+\lambda x^2)^{-1}$ which can be approximated using the binomial expansion. Considering only the first three terms of the binomial expansion of $(1+\lambda x^2)^{-1}$, we write Eq.(9) as

$$\ddot{x} - m_0(1-\lambda x^2+\lambda^2 x^4)(\gamma\lambda\, x\dot{x}^2 - \gamma\omega_0^2 x) + \gamma(1+\lambda x^2)(\alpha\dot{x} + \beta x^3) = \gamma(1+\lambda x^2)S(t) \tag{10}$$

After some mathematical manipulations given in ref.[32], Eq.(10) can be expressed in the form,

$$\ddot{x} - \lambda(x - \lambda x^3 + \lambda^2\, x^5)\dot{x}^2 + \alpha\gamma(1+\lambda x^2)\dot{x} + \omega_0^2\, x + \delta x^3 + \xi x^5 = \gamma(1+\lambda x^2)\; S(t), \tag{11}$$

where $\delta = \beta\gamma - \lambda\omega_0^2$ and $\xi = \beta\gamma\lambda + \lambda^2\omega_0^2$. Eq.(11) is also known as the PDM-Duffing oscillator equation. The corresponding potential of the system is

$$V(x) = \frac{\omega_0^2}{2}\, x^2 + \frac{\delta}{4}\, x^4 \; + \frac{\xi}{6}\, x^6 \; . \tag{12}$$

In our current study, we have selected specific mass parameter regimes that result in a double-well system potential. These regimes are characterized by $0 < m_0 < 1.5$ and $0 < \lambda < 1$, with fixed values of $\alpha = 0.2$, $\omega_0^2 = -1$, $\beta = 1$, and $f = 0.05$. The system potential, as depicted in Figures 1(a) and 1(b), corresponds to different combinations of the position-dependent mass (PDM) parameters: mass amplitude m_0 (values of 0.5, 1.5, 2.0, 4.0) with λ held constant at 1.0, and the strength of spatial nonlinearity in mass λ (values of 0, 1.0, 1.5, 2.0) with m_0 fixed at 1.0. This potential is computed using Eq. (12). It is noteworthy that a recent study by Suddalai Kannan et al. [34] investigated and analyzed the vibrational resonance (VR) phenomenon in a double-well position-dependent mass (PDM)-Duffing oscillator system driven by an amplitude-modulated signal. In contrast, our present work focuses on the numerical analysis of VR in a double-well PDM-Duffing oscillator system subjected to a frequency-modulated (FM) signal

4. **Analysis of Vibrational Resonance**

In this section, we analyze the existence of VR in the system (Eq.11) with NBFM and WBFM signals. To determine VR, we use the amplitude of the response at the frequency ω of the signal. Indeed, using the fourth-order Runge-Kutta method with time step size, we numerically integrate the system Eq.(11) under consideration. Thus the numerical solution of $x(t)$ allows to calculating the amplitude response Q through the following formula

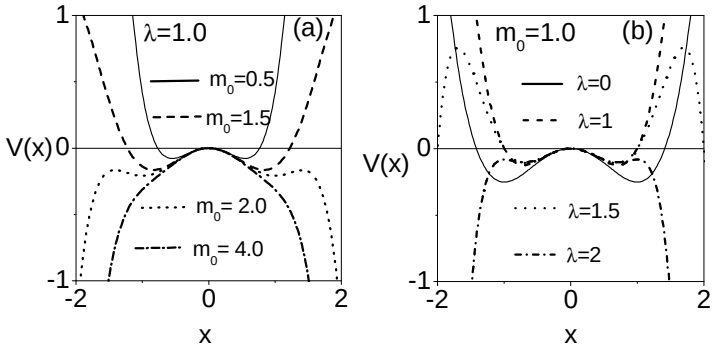

FIGURE 1. Shape of the potential $V(x)$ for (a) $\lambda = 1.0, m_0 = 0.5, 1.5, 2.0, 4.0$ (b) $m_0 = 1.0, \lambda = 0, 1.0, 1.5, 2.0$. The values of the other parameters are $\beta = 1$ and $\omega_0^2 = -1$.

$$Q_s = \frac{2}{nT}\int_0^{nT} x(t)\sin(\omega t)dt \tag{13a}$$

$$Q_c = \frac{2}{nT}\int_0^{nT} x(t)\cos(\omega t)dt \tag{13b}$$

with $T = 2\pi/\omega$ is the period of the response and n is taken as 200. Then,

$$Q = \frac{\sqrt{Q_s^2 + Q_c^2}}{f} \tag{13c}$$

In all the calculations, the initial conditions are chosen as $x(0) = 0.1$ and $\dot{x}(0) = 0$. The values of the system parameters are $\alpha = 0.2, \beta = 1, \omega_0^2 = -1$ and $f = 0.05$. The aim of the present work is to make the resonance appear or disappear through adjusting the signal parameters (g, ω, Ω) and the PDM parameters (m_0, λ).

4.1. **VR in PDM-Duffing system with NBFM signal.** Under the excitation of NBFM signal, the PDM-Duffing oscillator is described by the following equations

$$\dot{x} = y \tag{14a}$$

$$\dot{y} = \lambda(x - \lambda x^3 + \lambda^2 x^5)\dot{x}^2 - \alpha\gamma(1 + \lambda x^2)\dot{x} - \omega_0^2 x - \delta x^3 - \xi x^5 + \gamma(1 + \lambda x^2) S_1(t), \tag{14b}$$

We begin by examining the presence of VR in the system using Eq.(14), assuming a constant mass, denoted as $m(x) = m_0$, and setting λ to zero. Figure 2 illustrates the variation of Q concerning the parameter g and the influence of the parameters m_0, ω, and Ω. In Figure 2(a), we plot Q against g for three different values of m_0 (namely, 0.5, 1.0, and 1.5), while keeping λ at 0, ω at 0.75, and Ω at 15.0. For $m_0 = 0.5$ and 0.75, resonance does not occur when $g < 76.5$ and $g < 151.3$, respectively. However, when $g > 76.5$ for

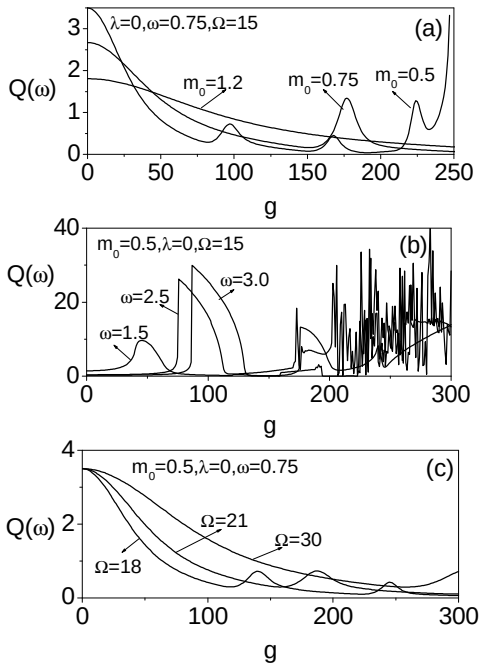

FIGURE 2. The response amplitude Q as a function of the amplitude of the high-frequency (g) component of the NBFM signal for different values of (a) $m_0 = (0.5, 0.75, 1.2)$ with $\lambda = 0, \omega = 0.75, \Omega = 15$ (b) $\omega = (1.5, 2.5, 3.0)$ with $\lambda = 0, m_0 = 0.5, \Omega = 15$ (c) $\Omega = (18, 21, 30)$ with $\lambda = 0, m_0 = 0.5, \omega = 0.75$. The values of the other parameters are $\beta = 1, \omega_0^2 = -1$ and $f = 0.05$.

$m_0 = 0.5$ and $g > 151.3$ for $m_0 = 0.75$, three resonance peaks appear for the former and a single resonance peak for the latter. Conversely, for $m_0 = 1.2$, the value of Q continuously decreases as g varies, and no resonance occurs. From Figure 2(a), it is evident that the number of resonance peaks decreases with an increase in m_0. The influence of ω on the observed resonance is presented in Figure 2(b), with λ set to 0, m_0 at 0.5, and Ω at 15.0. As the frequency of the low-frequency signal, ω, increases, enhanced VR becomes apparent for all values of ω. For $\omega = 1.5$, 2.0, and 3.0, the first resonance peak occurs in the interval $0 < g < 159.5$. Furthermore, beyond this interval, multiple resonance peaks appear for all values of ω as shown in Figure 2(b). Specifically, for $\omega = 1.5$, 2.0, and 3.0, the first resonance peak occurs at $g = g_{VR} = 50.5$ with $Q_{max} = 10.3$, $g = g_{VR} = 80.5$ with $Q_{max} = 25.5$, and $g = g_{VR} = 97.5$ with $Q_{max} = 30.3$, respectively. As ω increases, both Q_{max} and the peak position shift in the direction of increasing ω. In Figure 2(c), we explore the impact of the frequency of the high-frequency signal, Ω, on the observed resonance for $m_0 = 0.5$ and $\omega = 0.75$. For $\Omega = 30$,

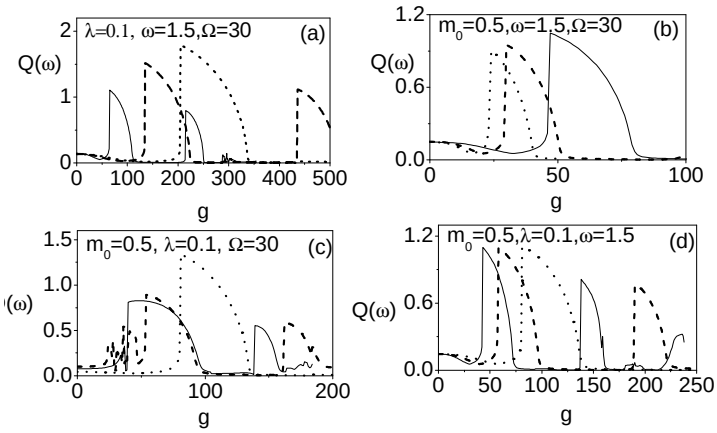

FIGURE 3. The response amplitude Q as a function of the amplitude of the high-frequency (g) component of the NBFM signal for different values of (a) $m_0 = 0.5$(solid line), 1.0(dashed line),1.5(dotted line)(b) $\lambda = 0.2$(solid line), 0.5(dashed line),0.7(dotted line) (c) $\omega = 0.75$(solid line), 1.0 (dashed line), 2.0(dotted line) (d) $\Omega = 21$(solid line), 27(dashed line), 36 (dotted line). The values of the other parameters are $\beta = 1, \omega_0^2 = -1$ and $f = 0.05$.

as g increases, Q decreases, and resonance is not observed. However, for $\Omega = 18$, two resonances are found at $g = 125.2$ and $g = 181.5$. In contrast, for $\Omega = 21$, only one resonance is found at $g = 249.5$. From Figure 2, it is clear that the VR phenomenon can be enhanced by adjusting the parameters of the PDM and the signal.

Additionally, when we activate the spatial nonlinearity parameter λ of the mass and examine the dependence of Q on m_0, ω, and Ω, the results are presented in Figure 3. Figure 3(a) illustrates the response curves that show the relationship between the response amplitude Q and the amplitude g of the high-frequency signal. This analysis is conducted for $\lambda = 0.1, \omega = 1.5, \Omega = 30$, and three different values of $m_0 = 0.5, 1, 1.5$. From Figure 3(a), it is evident that the maximum response amplitude Q increases as m_0 increases. Double resonances are observed for $m_0 = 0.5$ and 1.0, whereas a single resonance is found for $m_0 = 1.5$. To investigate the impact of the mass spatial nonlinearity parameter λ on the system's response, we depict the relationship between the response amplitude Q and the amplitude g of the high-frequency signal for three values of $\lambda = 0.2, 0.5, 0.7$ in Figure 3(b). The values of the other parameters are kept constant at $m_0 = 0.5, \omega = 1.5$, and $\Omega = 30$. The shape of the resonance curve and the maximum response amplitude Q_{max} are both influenced by λ. It is observed that the maximum response amplitude Q_{max} at which VR occurs increases with a greater strength of spatial nonlinearity in the mass, as shown in Figure 3(b).

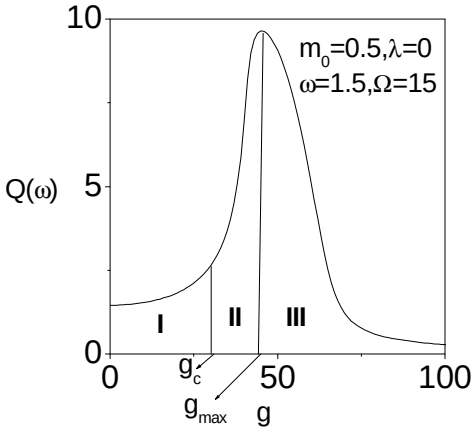

FIGURE 4. Dependence of the response amplitude Q on g for $\beta = 1, \omega_0^2 = -1$ and $f = 0.05$.

In our previous discussions, we established that the VR phenomenon can manifest in PDM parameters such as m_0 and λ. Now, we proceed to confirm the presence of the VR phenomenon in the context of the driving signal frequencies, namely (ω, Ω). In Figure 3(c), we depict the relationship between the response amplitude, Q, and the amplitude of the high-frequency signal, g, for three different values of ω $(0.75, 1.0, 2.0)$ while keeping $m_0 = 0.5$, $\lambda = 0.1$, and $\Omega = 30$. It is worth noting that in Figure 3(c), double resonances occur for $\omega = 0.75$ and $\omega = 2.0$. However, for $\omega = 1.0$, multiple resonance peaks emerge in the range $0 < g < 48.5$, followed by double resonances beyond this interval. These multiple resonance peaks are induced by the high-frequency harmonic driving. Finally, we investigate the impact of the frequency of the high-frequency component, Ω, on VR. The resonance curves are presented in Figure 3(d) for three different values of Ω $(21, 27, 36)$ while keeping $\omega = 0.5$, $\lambda = 0.1$, and $m_0 = 0.5$. Double resonances are observed for $\Omega = 21$ and $\Omega = 27$, while a single resonance occurs for $\Omega = 36$. The values of Q_{max} for the first and second resonances are nearly identical across all the values of Ω. However, as Ω increases, both g_{max} and the width of the resonance curves increase.

Figure 4 provides an explanation for the enhancement of resonance due to the mass amplitude m_0. In this figure, the plot is divided into three regions: region-I $(0 < g < 30.7)$, region-II $(30.7 < g < 45.8)$, and region-III $(45.8 < g < 100)$. As g increases from region-I, the response amplitude Q increases, reaching its maximum value at $g = g_{max} = 45.8$ in region-II, but then decreases with further increases in g in region-III. Figures 5 and 6 present the phase portraits and trajectory plots corresponding to the regions in Fig. 4. In all three regions, the motion is periodic with a period of $T = 2\pi/\omega$. In region-I $(0 < g < 30.7)$, each periodic orbit remains confined to one well without cross-well motion (Figs. 5(a) and 6(a)). In this region,

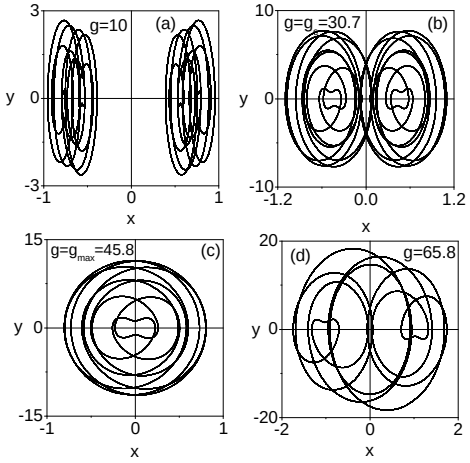

FIGURE 5. Phase portraits for different values of high-frequency amplitude g. The other parameters are fixed at $m_0 = 0.5, \lambda = 0, \omega = 1.5, \Omega = 15, \beta = 1, \omega_0^2 = -1$ and $f = 0.05$.

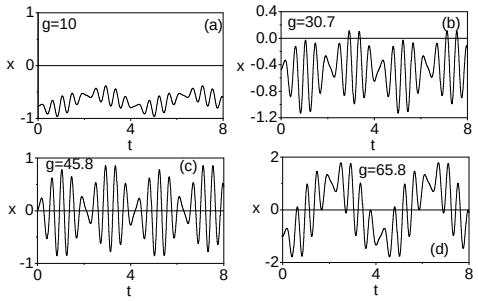

FIGURE 6. Trajectory plots for few values of g. The other parameters are fixed at $m_0 = 0.5, \lambda = 0, \omega = 1.5, \Omega = 15, \beta = 1, \omega_0^2 = -1$ and $f = 0.05$.

the response amplitude Q increases smoothly and gradually with increasing g. When $g = 30.7$, cross-well motion begins, and the trajectory spends relatively little time in the regions $x < 0$ and $x > 0$. This dynamic behavior characterizes region-II, as seen in Figs. 5(b) and 6(b). In this region, there is a rapid increase in amplitude Q and region-II is quite narrow. Although the period of the orbit in region-III is still T, its shape differs from those in regions I and II. Fig. 5(c) illustrates the phase portrait of the period-T orbit for $g = 45.8$, while the corresponding trajectory plot is shown in Fig. 6(c). In region-III, as g increases, the response amplitude Q reaches its maximum value at $g = g_{max} = 45.8$, significantly enhancing the weak signal. Both figures 5(c) and 6(c) illustrate that the PDM parameters can enhance VR and improve the weak low-frequency signal in the system. When

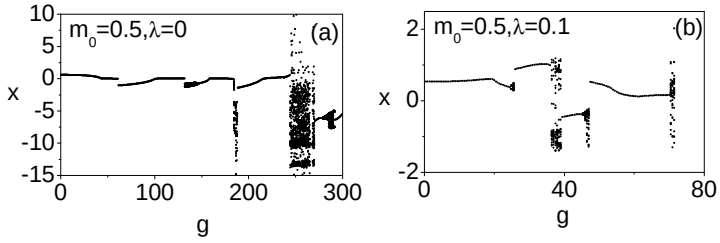

FIGURE 7. Bifurcation diagrams of the system (Eq.11) with (a) $\lambda = 0$ and (b) $\lambda = 0.1$. The other parameters are fixed at $m_0 = 0.5, \omega = 1.5, \Omega = 15, \beta = 1, \omega_0^2 = -1$ and $f = 0.05$.

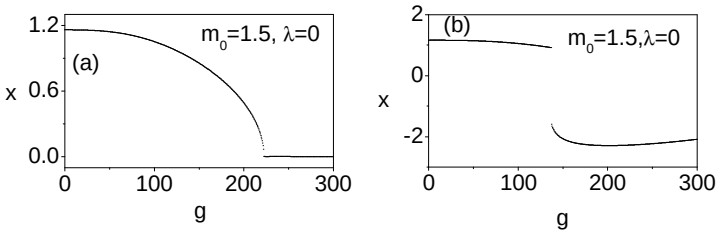

FIGURE 8. Bifurcation diagrams of the system (Eq.11). Here $m_0 = 1.5, \lambda = 0, \omega = 1.5, \Omega = 15, \beta = 1, \omega_0^2 = -1, f = 0.05$ and g is varied in the forward direction in (a) while it is decreased from a large value to small value in (b).

g increases above g_{max}, the response amplitude Q gradually decreases and eventually decays to zero. The corresponding phase portrait and trajectory plot for $g = 65.8$ (far from the resonance) are shown in Figs. 5(d) and 6(d). These two figures can be compared with the phase portrait and trajectory plot of orbits in regions I and II, revealing a different orbit shape in this case. The bifurcation diagram of the PDM-Duffing oscillator system, with and without the mass spatial nonlinearity parameter λ for $m_0 = 0.5$, is presented in Figs. 7(a) and 7(b). These diagrams display stable periodic orbits, period-doubling, reverse period-doubling, attractor crises, and chaotic dynamics. After introducing the mass spatial nonlinearity parameter λ the chaotic orbit is significantly suppressed, as clearly shown in Fig. 7(b).

4.2. **Hysteresis phenomenon.** Figures 8(a) and 8(b) depict the bifurcation diagram obtained by varying the parameter g in the forward and reverse directions, respectively. We have maintained the values of the other parameters as constants, specifically $\omega = 1.5$, $\Omega = 15$, $\alpha = 0.2$, $\beta = 1.0$, $\omega_0^0 = -1$, and $f = 0.05$. In this bifurcation diagram, the ordinate represents the values of $x(t)$ recorded at time intervals equal to every integral multiple of $2\pi/\omega$ (referred to as Poincaré points) after allowing sufficient time for system evolution. Figures 8(a) and 8(b) reveal different trajectories. These figures

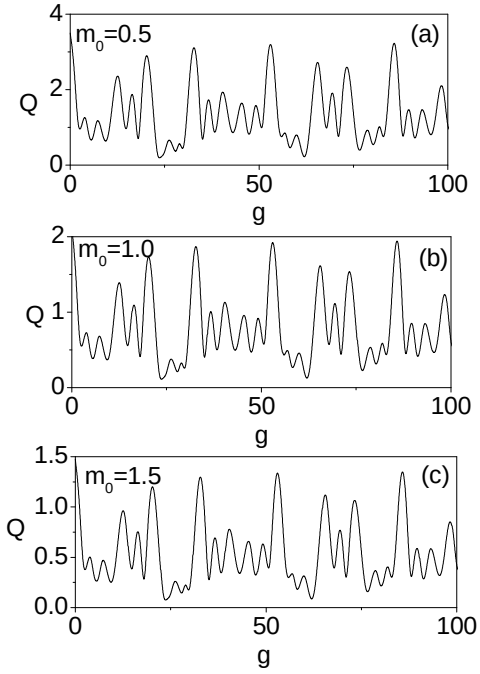

FIGURE 9. The response amplitude Q as a function of the amplitude of the high-frequency (g) component of the WBFM signal for different values of (a) $m_0 = 0.5$ (b) $m_0 = 1.0$ (c) $m_0 = 1.5$. The values of the other parameters are $\beta = 1, \omega_0^2 = -1, \omega = 0.75, \Omega = 15, \lambda = 0$ and $f = 0.05$.

illustrate that the system exhibits a hysteresis phenomenon as the control parameter g is smoothly varied from a small value to a larger one and then back to a small value.

4.3. **VR in PDM-Duffing system with WBFM signal.** In the preceding section, we examined the occurrence of VR using an NBFM signal within the system described by Eq. 11, considering various PDM and signal parameters. In this section, we undertake a numerical analysis to investigate the presence of vibrational resonance in the PDM-Duffing oscillator system (governed by Eq. 11) driven by a WBFM signal. When subjected to the excitation of a WBFM signal, the dynamics of the PDM-Duffing oscillator are described by the following equations

$$\dot{x} = y \tag{15a}$$

$$\dot{y} = \lambda(x - \lambda x^3 + \lambda^2 x^5)\dot{x}^2 - \alpha\gamma(1 + \lambda x^2)\dot{x} - \omega_0^2 x - \delta x^3 - \xi x^5 + \gamma(1 + \lambda x^2) S_2(t), \tag{15b}$$

First, we conduct a numerical analysis to examine the occurrence of Vibrational Resonance (VR) in the system described by Eq.(15) with a fixed

mass amplitude (m_0), i.e., without considering the mass spatial nonlinearity parameter ($\lambda = 0$). The results are presented in Figure 9. In Figure 9, we depict the response amplitude Q as a function of the amplitude g of the fast signal in the range $g \in [0, 100]$. We maintain $\omega = 0.75$, $\Omega = 15.0$, and keep other parameters constant, as previously defined. In this figure, we investigate the influence of the mass amplitude m_0 with values of m_0 set to 0.5, 1.0, and 1.5, respectively, on VR using numerical simulations. As illustrated in the figure, multiple resonances are observed for all values of m_0, and as m_0 increases, the maximum response amplitude (Q_{max}) decreases. Figure 10 examines the role of mass spatial nonlinearity parameter λ on the VR effect. The conclusion is consistent with that in the system with a fixed mass amplitude m_0 (i.e., $\lambda = 0$), indicating that Q_{max} of VR decreases as m_0 increases.

Now, we turn our attention to explaining the underlying dynamics associated with the occurrence of resonances. To facilitate this, we find it highly convenient to utilize time series and phase space plots. Figures 11 and 12 provide insights into the behavior of the response when g falls within the resonance region, considering cases with $m_0 = 0.5$, 1.5, and $\lambda = 0$. For

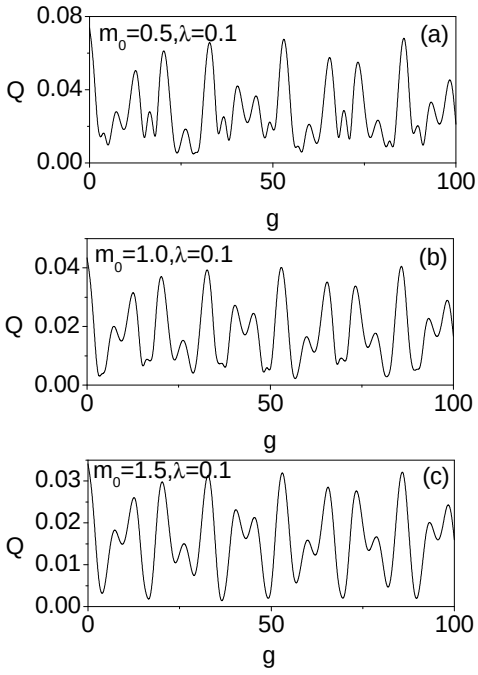

FIGURE 10. The response amplitude Q as a function of the amplitude of the high-frequency (g) component of the WBFM signal for different values of (a) $m_0 = 0.5$ (b) $m_0 = 1.0$ (c) $m_0 = 1.5$. The values of the other parameters are $\beta = 1, \omega_0^2 = -1, \omega = 0.75, \Omega = 15, \lambda = 0.1$ and $f = 0.05$.

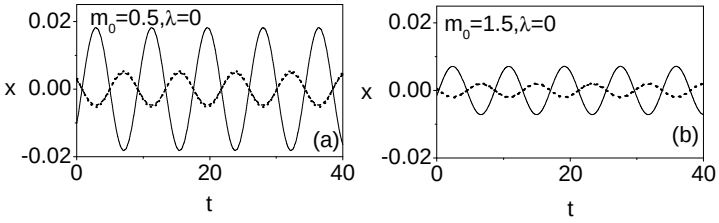

FIGURE 11. Trajectory plots for few values of g chosen in the resonant regions in Fig.9(a). The corresponding parameters are the same as those in Fig.9(a).

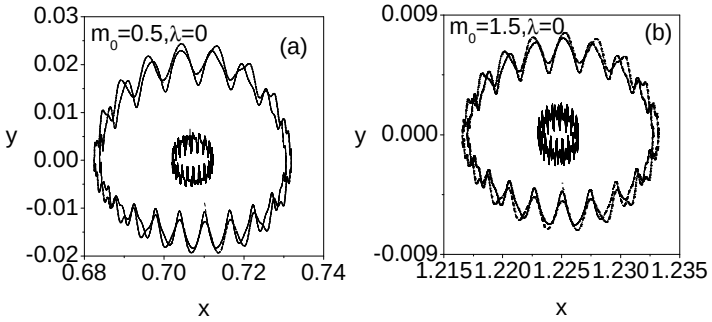

FIGURE 12. Phase portraits for a few values of high-frequency amplitude g chosen in the resonant regions in Fig.9(a). The corresponding parameters are the same as those in Fig.9(a).

$m_0 = 0.5$, as illustrated in Figure 11(a), the response trajectories, represented by solid, dashed, and dotted lines, correspond to different values of g within the resonant regions shown in Figure 9(a). These trajectories reveal that the displacement of the particles modulates as m_0 increases. The corresponding phase portraits, as shown in Figure 12(a), confirm the monotonic increase in the size of the periodic orbit. As another example of this scenario, we present in Figures 11(b) and 12(b) the effect of the response amplitude for $m_0 = 1.5$ and $\lambda = 0$. In this case, the amplitude of the high-frequency signal, g, increases from 0 to 100, leading to modulation in the particle displacement amplitudes, as depicted in the time series plot in Figure 11(b). Correspondingly, a monotonic increase in the size of the periodic orbit is evident in the phase portrait shown in Figure 12(b).

5. Conclusion

In this study, we conducted numerical investigations to explore the impact of frequency-modulated (FM) signals on vibrational resonance (VR) within a position-dependent mass (PDM)-Duffing oscillator system. FM signals were

categorized into two main types: narrow-band FM (NBFM) and wide-band FM (WBFM) signals. Our numerical simulations have revealed that PDM parameters exert a significant influence on VR, allowing for the suppression, induction, or modulation of vibrational peaks. The use of FM signals has demonstrated its potential to control a variety of complex phenomena. Beyond the dynamic changes, which include period-doubling splitting, inverse period-doubling splitting, crises, and chaotic orbits, we have observed a multitude of resonance peaks, an enhancement in response amplitude $Q(\omega)$, the persistence of non-decaying $Q(\omega)$, as well as intriguing behaviors such as hysteresis and a jump phenomenon. Remarkably, these effects persist even for large values of PDM and signal parameters.

Exploring the influence of FM signals and pulse-modulated signals on various types of systems, as well as their interaction with various external forces, holds promise for yielding fascinating and novel results in the field of dynamic systems research.

References

[1] P.S. Landa, and P.V.E. McClintock, Vibrational Resonance, J. Phys. A, 33 (2000) 1433-8.

[2] M. Gitterman, Bistable oscillator driven by two periodic fields, J. Phys.A, 34 (2001) 355-7.

[3] I.I. Blekhman, and P.S. Landa, Conjugate resonances and bifurcations in nonlinear systems under biharmonical excitation, Int. J. Nonlin. Mech., 39 (2004) 421-426. (doi:10.1016/S0020-7462(02)00201-9

[4] S. Jeyakumari, V. Chinnathambi, S. Rajasekar, and M.A.F. Sanjuan, Single and multiple vibrational resonance in a quintic oscillator with monostable potentials, Phys. Rev.E, 80 (2009) 046608.

[5 S. Jeyakumari, V. Chinnathambi, S. Rajasekar, and M.A.F. Sanjuan, Analysis of vibrational resonance in a quintic oscillator, Chaos, 19 (2009) 043128-8.

[6] S. Huang, J. Zhang, J. Yanga, H. Liu, and M.A.F. Sanjuán, Logical vibrational resonance in a symmetric bistable system: Numerical and experimental studies, Communications in Nonlinear Science and Numerical Simulation, 119 (2023) 107123.

[7 R. Gui, T. Wang, Y. Yao, and G. Cheng, Enhanced logical vibrational resonance in a two-well potential system, Chaos, Solitons & Fractals, 138 (2020) 109952

[8] T. Zhang, Y. Jin, Y. Xu, and X. Yue, Dynamical response and vibrational resonance of a tri-stable energy harvester interfaced with a standard rectifier circuit, Chaos, 32 (2022) 093150. https://doi.org/10.1063/5.0105337.

[9] B. Bhuvaneshwari, K. Amutha, V. Chinnathambi, and S. Rajasekar, Enhanced vibrational resonance by an amplitude modulated signal in a nonlinear dissipative two-fluid plasma model, Contributions to Plasma Physics, e202100099, (2021) 1-10,

[10] B. Bhuvaneshwari, S. Valli Priyatharsini, V. Chinnathambi, and S. Rajasekar, Vibrational resonance in two-dimensional nonlinear maps, Chaotic Modeling and Simulation (CMSIM), 3 (2021) 179- 90.

[11] E.I. Volkov, E. Ullner, A. Zaikin, and J. Kurths, Oscillatory amplification of stochastic resonance in excitable systems, Phys. Rev.E, 68 (2003) 026214.

[12] A.O. Maksimov, On the subharmonic emission of gas bubbles under two-frequency excitation, Ultrasonics, 35 (1997) 79-86.

[3 J. Victor, and M. Conte, Two-frequency analysis of interactions elicited by vernier stimuli, Visual Neurosci., 17 (2000) 959-973.

[14] V.E. Gherm, N.N. Zernov, B. Lundborg, and A. Vastberg, A., The two-frequency coherence function for the fluctuating ionosphere; narrowband pulse propagation, J. Atmos.Sol-Terr. Phys., 59 (1997) 183.
[5 C.W. Cho, Y. Liu, W.N. Cobb, T.K. Henthom, K. Lillenei, U. Christians, and K. Ng, Ultrasound-induced mild hyperthermia as a novel approach to increase drug uptake in brain microvessel endothelial cells, Pharm. Res., 19 (2002) 1123-1129.
[16] J.L. Karnes, and H.W. Burton, Continuous therapeutic ultrasound accelerates repair of contraction-induced skeletal muscle damage in rats, Arch. Phys. Med. Rehabil., 83 (2002) 1-4.
[7 O.'Schalfer, T. Onyecha, H. Bormann, C. Schroder, and M. Sievers, Ultrasonics, 40 (2002) 25.
[8 R. Feng, Y. Zhao, C. Zhu, and T.J. Mason, Enhancement of ultrasonic cavitation yield by multi-frequency sonication, Ultrason Sono Chem., 9 (2002) 231-236.
[9 A. Pratim Ghosh, A. Mandal, S. Sarkar, M. Ghosh, Influence of position-dependent effective mass on the nonlinear optical properties of impurity doped quantum dots in presence of Gaussian white noise, Opt. Commun., 367 (2016) 325-334.
[20] Q. Zhao, et al. Influence of position-dependent effective mass on the nonlinear optical properties in $Al_xGa_{1-x}As/GaAs$ single and double triangular quantum wells, Physica E, 115 (2020) 113707.
[21] H. Irschik and A.K. Belyaev, eds. Dynamics of mechanical systems with variable mass, vol.557 of CISM International Centre for Mechanical Sciences, 2014, Germany: Springer-Verlag Wien, 1 edn
[22] K.S. Krane, The falling raindrop: variations on a theme of Newton, Amer. J. Phys., 49 (1981) 113-117.
[23 N. Aquino, G. Campoy, and H. Yee-Madeira, The inversion potential for NH3 using a DFT approach, Chem. Phys. Lett., 296 (1996) 111-116.
[24] M.R. Bate, Predicting the properties of binary stellar systems: the evolution of accreting protobinary systems, Mon. Not. R. Astron. Soc., 314 (2000) 33-53.
[25 H.A. Bethe, Possible explanation of the solar-neutrino puzzle, Phys Rev Lett., 56 (1986) 1305-8. (https://doi.org/10.1201/9780429502811-95)
[26] P.M. Mathews, and M. Lakshmanan, On a unique nonlinear oscillator, Quart. Appl. Math., 32 (1974) 215-218.
[27 R. Bravo, and M.S. Plyushchay, Position-dependent mass, finite-gap systems, and supersymmetry, Phys. Rev. D, 93 (2016) 105023.
[28 V. Bala Shunmuga Jothi, S. Selvaraj, V. Chinnathambi, and S. Rajasekar, Chaos, hysteresis and vibrational resonance in a single scroll Chua's circuit driven by frequency modulated force, International Journal of Theoretical and Applied Physics (IJTAP), 7(1) (2017) 1-11.
[29 B. Bhuvaneshwari, S. Valli Priyatharsini, V. Chinnathambi, and S. Rajasekar, Dynamics of nonlinearly damped Duffing-vander Pol oscillator driven by frequency modulated signal, Nonlinear Dynamics and Systems Theory, 21(5) (2021) 1-10.
[30] O. Mustafa, Comment on nonlinear dynamics of a position-dependent mass-driven Duffing-type oscillator, J. Phys. A: Math. Theor., 46 (2013) 368001.
[31] S.C.Y. Cruz, and O. Rosas-Ortiz, Dynamical equations, invariants and spectrum generating algebras of mechanical systems with position-dependent mass, Symmetry Integr. Geom., 9 (2013) 4-21.
[32] T.O. Roy-Layinde, U.E. Vincent, S.A. Abolade, O.O. Popoola, J.A. Laoye, and P.V.E. McClintock, Vibrational resonances in driven oscillators with position-dependent mass, Phil. Trans. R. Soc. A, 379 (2020) 20200227. https://doi.org/10.1098/rsta.2020.0227.
[33] Y. Zhang, and S. Li, Combination and simultaneous resonances of gas bubbles oscillating in liquids under dual-frequency acoustic excitation, Ultrason. Sonochem, 35 (2017) 431-439.

[34] K. Suddalai Kannan, S.M. Abdul Kader, M.V. Sethu Meenakshi, V. Chinnathambi and S. Rajasekar, Nonlinear response of a position dependent mass system driven by an amplitude modulated force, Dynamic system and applications, 32 (2023) 18-32.

K. Suddalai Kannan[1], T. SaintaJoster[2], A. Zeenath Bazeera[3],V. Chinnathambi[4,*]
Department of Physics,
Sadakathullah Appa College,
Tirunelveli-627 011,
Tamilnadu,
India.
e-mails:[1]ksramar1992k@gmail.com, [2]saintajoster85@gmail.com, [3]meeran.jul1@gmail.com,
[4,*]Corresponding author:veerchinnathambi@gmail.com

S. Rajasekar[5]
School of Physics,
Bharathidasan University,
Tiruchirapalli 620 024,
Tamilnadu,
India.
[5]email:srj.bdu@gmail.com